Received 26 August 2025; Accepted 12 November 2025
https://doi.org/10.48612/letters/2025-4-336-343
https://elibrary.ru/lubxft

Enhancing high-temperature resistance of structural steels by forming nickel-based coatings via non-vacuum electron-beam cladding

P. M. Petukhova, E. G. Bushueva†, R. R. Nurdinov, B. B. Batyrov, D. O. Mul, E. A. Lozhkina

†dusias@mail.ru

Novosibirsk State Technical University, Novosibirsk 630073, Russia

Abstract: Nickel-based coatings were fabricated on 0.4 wt.% C-Cr structural steel substrates via non-vacuum electron beam cladding (NVEB cladding), using Colmonoy-227F self-fluxing powder. This study presents results on the microstructure and properties of single-, double-, and triple-layer coatings. The optimal electron beam current for the formation of defect-free alloyed coatings is 23 mA. The thickness of single-, double- and triple-layer coatings is 2.7 mm, 3.4 mm and 4.4 mm, respectively. The coatings have a dendritic structure with crystals of the first and second order. Microstructural analysis revealed that single- and double-layer coatings consisted primarily of a γ-FeNi substitutional solid solution. The application of a third layer led to precipitation of $Fe_{1.8}Ni_{1.2}P$ phosphide and $FeSi_2$ silicide phases. A decrease in iron content within the coating with an increasing number of layers was observed, which correlated with improved resistance to high-temperature oxidation. The paper presents the results of a comparative study of high-temperature oxidation in an air atmosphere at 850°C for 100 hours of 0.4 wt.% C-Cr steel and single-layer, double-layer and triple-layer nickel-based coatings. It was found that the weight gain of 0.4 wt.% C-Cr steel was 60.81 mg/m^2, while for the deposited coatings the values were significantly lower: 17.87 mg/m^2 (single-layer), 11.22 mg/m^2 (double-layer) and 7.01 mg/m^2 (three-layer). X-ray diffraction (XRD) analysis revealed that the oxide films formed on the deposited coatings consisted of iron oxides (Fe_3O_4, Fe_2O_3) and spinel $NiFe_2O_4$. A factor that increases resistance to high-temperature oxidation is the formation of protective spinel, which prevents the diffusion of oxygen and metal. Consequently, the triple-layer coating exhibited an 8.7-fold increase in resistance to high-temperature oxidation in air compared to the 0.4 wt.% C-Cr steel substrate alone.

Keywords: non-vacuum electron beam cladding, nickel-based coating, microstructure, high-temperature oxidation resistance, structural steel

Acknowledgements: *Research was conducted at core facility "Structure, mechanical and physical properties of materials". The work was carried out in accordance with the state task of the Ministry of Education and Science of Russia (project FSUN-2023-0009).*

1. Introduction

Enhancing the oxidation resistance of structural materials at high temperatures is a crucial objective in modern materials science. In particular, components made from 0.4 wt.% C-Cr steel are typically used under moderate loads at temperatures not exceeding 450 – 500°C. Above these temperatures, surface oxidation accelerates, leading to significant scale formation and degradation of mechanical properties [1]. Initially, oxidation of iron-containing components leads to the formation of a thin, well-adhered layer of wüstite (FeO). Further oxidation results in the formation of a thicker, less dense layer of magnetite (Fe_3O_4) covering the wüstite. Subsequent exposure to high temperatures promotes the formation of a porous and brittle hematite layer (Fe_2O_3), which spalls readily, accelerating the oxidation process. The formation of hematite, in particular, significantly increases the oxidation rate and promotes material degradation [2]. Therefore, the development and implementation of effective materials and methods for improving the high-temperature oxidation resistance of structural steels is an important area of research for extending component service life in high-temperature environments without significantly increasing production costs.

To address this challenge, significant research is focused on the development and application of alloys capable of effectively resisting high-temperature degradation under aggressive service conditions. Nickel-based alloys are widely employed due to their inherent corrosion resistance and high-temperature oxidation resistance [3, 4]. The oxidation of nickel in the temperature range of 700 – 900°C follows a sub-parabolic rate law, which is attributed to the diffusion-limited transport of oxygen through the growing oxide scale. The morphology of the oxide scale directly influences this diffusion process. These scales are typically characterized by a fine-grained microstructure with lamellar features and acicular crystals. At temperatures exceeding 1100°C, the oxidation kinetics of nickel follows a parabolic law. The oxide scales formed at these higher temperatures consist of columnar grains that extend throughout the entire scale

thickness [5]. Thus, nickel alloys represent a promising class of structural materials exhibiting high resistance to high-temperature oxidation on the work surface.

Manufacturing entire components from nickel-based alloys can be cost-prohibitive. Therefore, functional coatings are often applied to reduce product cost while maintaining performance characteristics. Furthermore, the development of easily repairable coatings to address inevitable degradation during service is an important consideration.

Modern surface modification technologies, such as thermal spraying [6–8], laser processing [9–11], and physical or chemical vapor deposition (PVD/CVD) [12–14], can significantly improve the to high temperature oxidation resistance of materials. Non-vacuum electron beam cladding (NVEB cladding) is of particular interest due to its ability to produce coatings with good adhesion and thicknesses up to 10 mm. NVEB cladding also allows for the fabrication of multiple layers and the incorporation of refractory elements. The elimination of the need for a vacuum environment makes this method economically attractive and technologically straightforward [15,16]. Colmonoy-227F, a nickel-based alloy in the Ni-P-Si-B system, is a promising material for protective coatings in high-temperature and abrasive wear environments. This alloy exhibits high-temperature oxidation resistance, corrosion resistance, and excellent anti-friction properties, making it particularly effective for such applications.

When nickel-containing coatings are formed on steel, not only the powder composition, but also the base material melts during non-vacuum electron beam surfacing, which leads to iron entering the melt bath and leads to nickel dilution with iron. A high iron concentration can negatively impact the oxidation resistance of nickel alloys due to the formation of a multi-layered oxide scale. However, under high-temperature exposure to the Fe-Ni system, spinel $NiFe_2O_4$ is formed, which exhibits high stability and serves as an effective barrier to oxygen diffusion into the bulk material, can form under high-temperature conditions in the Fe-Ni system [17]. To minimize the iron concentration in the coating, the deposition of multiple nickel-containing layers is recommended.

Therefore, the purpose of this study is to produce a multi-layered, high-temperature oxidation-resistant nickel coating on 0.4 wt.% C-Cr structural steel.

2. Materials and methods

Plates with dimensions of 100 × 50 × 12 mm, fabricated from 0.4 wt.% C-Cr (AISI 5140) structural steel (0.36 wt.% C, 0.90 wt.% Cr, 0.25 wt.% Si, 0.60 wt.% Mn, 0.03 wt.% P, 0.02 wt.% S, 0.17 wt.% Ni, 97.67 wt.% Fe), were used as the substrate material. Colmonoy-227F self-fluxing nickel-based powder was used for coating formation. Energy dispersive X-ray analysis revealed that the chemical composition of Colmonoy-227F powder includes: 3.11 wt.% Si, 3.55 wt.% P, 0.89 wt.% B, 92.75 wt.% Ni. Silicon, phosphorus and boron are introduced to form a thin glassy film when heated, protecting the molten metal from atmospheric oxidation. The powder is characterized by predominantly spherical particle morphology with particle sizes ranging from 20 to 100 μm (Fig. 1). The mass of powder surfaced was 0.45 g per 1 cm^2 of the base material.

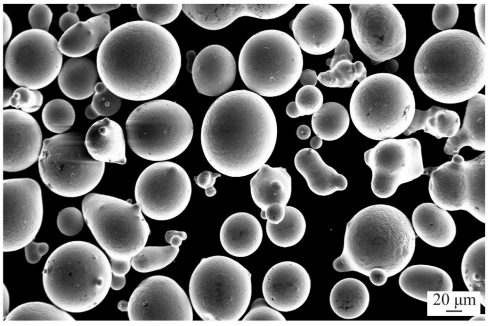

Fig. 1. Morphology of Colmonoy-227F powder particles.

The non-vacuum electron beam cladding process was performed at the Budker Institute of Nuclear Physics (INP), SB RAS. The processing parameters were as follows: electron beam current — 17, 20, and 23 mA; electron beam energy — 1.4 keV; scanning speed — 10 mm/s; and specific surface energy — 6.44 kJ/cm^2. The description of this method is presented in more detail in the following literature [18–20].

Microstructural characterization was conducted using a Carl Zeiss Axio Observer A1m optical microscope and a Carl Zeiss Merlin scanning electron microscope (SEM). Local chemical composition analysis was performed using an EDS X-Act microanalyzer. X-ray diffraction (XRD) analysis was carried out on an ADVIN PowDix600 diffractometer using CuKα radiation in step-scanning mode with a step size of 0.05°. Phase identification from the X-ray diffraction patterns was performed using the ICDD PDF-4 database.

High-temperature oxidation resistance tests were conducted according to GOST 6130-71. Samples for high-temperature oxidation testing were prepared from the coatings using wire electrical discharge machining (WEDM). The sample dimensions were 20×15×1 mm. Oxidation of the samples was performed in alumina crucibles with lids. High-temperature oxidation testing of the coatings and substrate material was carried out at 850°C for 100 hours in a muffle furnace in an air atmosphere. The samples, together with crucibles, were weighed every 12 hours using a GOSMETR VL-124V analytical balance with an accuracy of 0.1 mg. The morphology and elemental composition of the sample surfaces after high-temperature oxidation were analyzed using scanning electron microscopy (SEM) and X-ray microanalysis. The oxidation kinetics of the coatings and substrate material were determined by measuring the mass gain, Δm. The mass gain value was calculated as follows:

$$\Delta m = \Delta w / s,$$

where Δw is the change in sample mass (g); s is the initial sample area (cm^2).

Following the oxidation tests, the phase composition of the oxide scale was analyzed using an X-ray diffractometer. The XRD analysis was performed with a step size of 0.05° and an exposure time of 2 s. Cross-sections of the coatings after oxidation were examined using a Carl Zeiss EVO 50 XVP scanning electron microscope (SEM) equipped with an Oxford Instruments X-Act energy-dispersive spectrometer (EDS).

3. Results and discussion

To produce high-quality, defect-free coatings, experiments were conducted to determine the optimal electron beam current. Considering that the melting point of Colmonoy-227F powder is approximately 1000°C, the initial experiments were performed using low electron beam current values of 17 and 20 mA, which theoretically provide surface heating temperatures of up to 1600°C and 1800°C, respectively.

The resulting coatings (Fig. 2), formed under these conditions, exhibited a significant number of structural defects. Specifically, the coatings produced with an electron beam current of 17 mA displayed increased porosity (Fig. 2 a). This phenomenon is attributed to the rapid solidification rate of the melt, which inhibits the escape of gas inclusions to the surface. Furthermore, an insufficient beam current can lead to incomplete melting of the material, thereby promoting the formation of gas pores and voids within the coating structure. These factors collectively have a detrimental effect on the mechanical and operational properties of the coating.

Coatings formed with an electron beam current of 20 mA were characterized by an increased tendency to crack formation (Fig. 2 b). The primary causes of defect formation were thermal stresses and the precipitation of brittle phases containing phosphorus and silicon.

The energy input at 20 mA was insufficient to ensure complete melting and homogenization of the melt, which promoted the formation of a non-homogeneous structure. Residual stresses concentrated in these regions, which, upon exceeding critical values, led to coating fracture. An additional factor exacerbating the cracking process is the mismatch in the coefficients of thermal expansion between the coating material and the substrate, which intensifies internal stresses at the interface.

Therefore, crack formation under these cladding conditions is a result of the interaction of thermal, microstructural, and processing parameters. Optimization of the electron beam processing parameters was required to improve the coating quality. It was hypothesized that further increasing the electron beam current would result in the formation of a defect-free coating.

Consequently, cladding with a beam current of 23 mA resulted in the formation of a defect-free coating with a thickness of 2.7 mm (Fig. 2 c).

The coating structure exhibited a dendritic morphology, which is a characteristic feature of rapid solidification from the molten state. Dendrite growth was oriented perpendicular to the substrate material due to heat extraction during the crystallization process [21].

Following the determination of the optimal electron beam current for a single-layer coating (23 mA), experiments were conducted to fabricate multi-layer coatings with two and three layers (Fig. 3).

The double-layer coating thickness ranged from 3 to 3.4 mm, while the triple-layer coating thickness ranged from 4 to 4.4 mm. Vertical cracks were observed in the triple-layer coating. The presence of these defects can be attributed to several factors: the accumulation of internal stresses at the interlayer boundaries; the non-uniform thermal cycles experienced during sequential layer cladding, and the disruption of diffusion processes between the cladded layers and the substrate material. Furthermore, the chemical composition difference between the coating and the substrate material contributes to residual

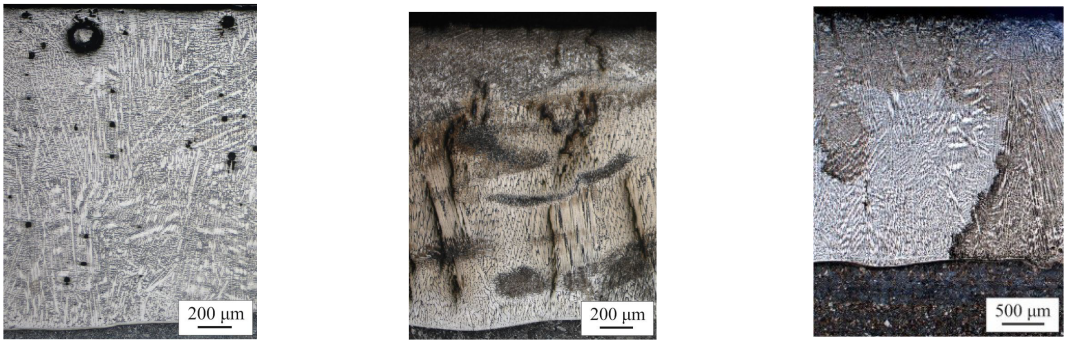

a b c

Fig. 2. (Color online) Cross section of deposited coatings based on Colmonoy-227F nickel alloy formed at different beam currents: 17 mA (a), 20 mA (b), 23 mA (c).

a b

Fig. 3. (Color online) Structure of surfaced coatings based on Colmonoy-227F nickel alloy, formed using multi-layer cladding: double-layer surfacing (a), triple-layer surfacing (b).

stresses, primarily due to the mismatch in the coefficients of thermal expansion [22].

Following cladding with Colmonoy-227F powder, the formation of brittle eutectic phases was observed within the coating structure, primarily localized in the interdendritic regions. This distribution is attributed to the segregation of phosphorus during melt crystallization, which lowers the liquidus temperature in these zones, leading to the subsequent formation of secondary phases during final solidification. These brittle phases render the intercrystalline zones particularly susceptible to residual tensile stresses arising from the non-uniform thermal cycles associated with cladding and the differences in the coefficients of thermal expansion between the coating material and the substrate material. Under the influence of residual tensile stresses, micropores formed in these regions, primarily in the interdendritic region (Fig. 4 b, d). Subsequently, crack propagation occurred via an interdendritic fracture mechanism through the coalescence of adjacent pores in a direction perpendicular to the tensile stress (Fig. 4 c, e).

It was observed that, regardless of the number of cladded layers, the coating structure exhibited a dendritic morphology. Figure 5 presents SEM micrographs illustrating the coating structure. Table 1 summarizes the results of local energy-dispersive X-ray (EDX) analysis, conducted to evaluate the elemental composition of both dendritic and interdendritic regions.

Notably, the phosphorus concentration increased in the interdendritic regions with an increasing number of layers. Furthermore, the fabrication of multi-layer coatings effectively reduced the extent of iron diffusion from the

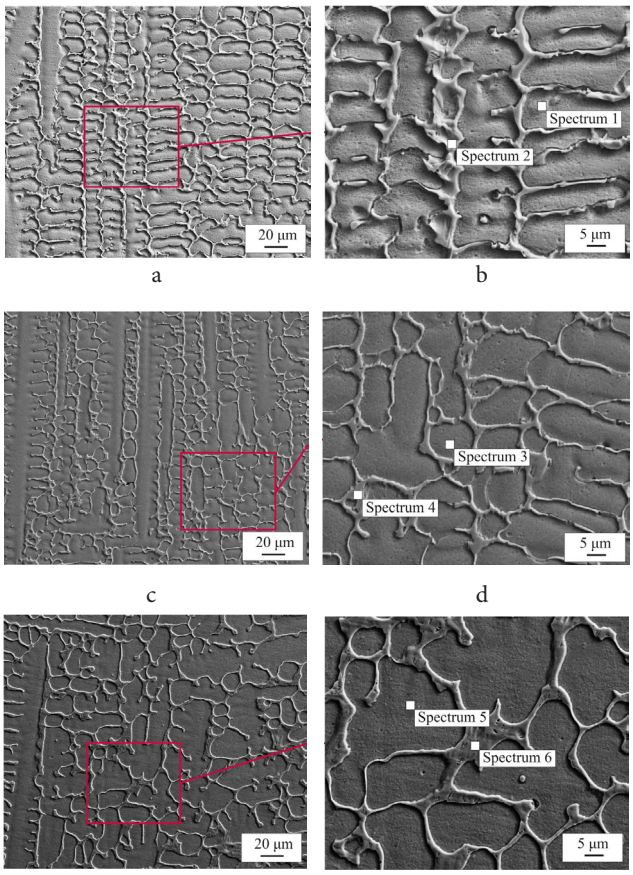

Fig. 5. SEM cross-sectional images of coatings based on Colmonoy-227 nickel alloy formed by multilayer cladding: single-layered (a, b), double-layered (c, d), triple-layered (e, f).

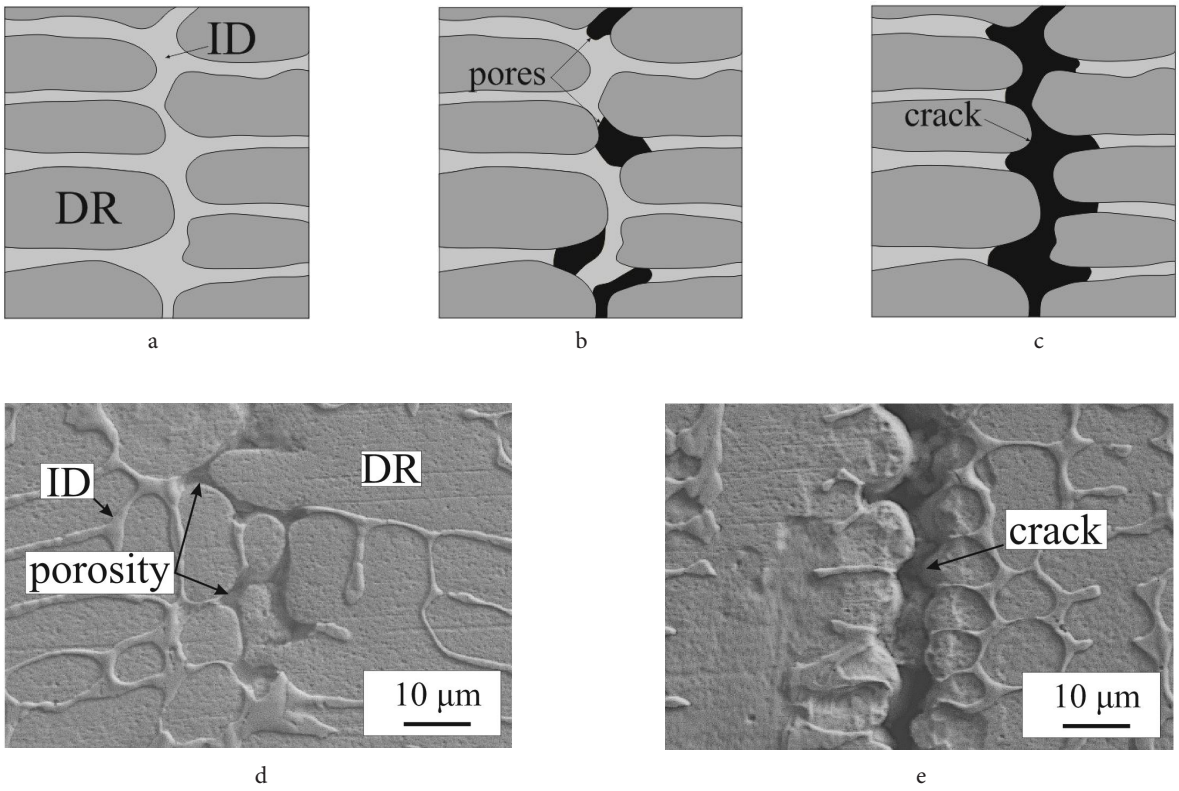

Fig. 4. Structural defects: patterns of crack development (a, b, c), pores in the structure of the material (d), cracks in the structure of the material (e). DR — dendritic region, ID — interdendritic region.

Table 1. EDX analysis of local coating zones, at.%.

Element	Spectrum 1	Spectrum 2	Spectrum 3	Spectrum 4	Spectrum 5	Spectrum 6
Si	2.84	–	2.63	–	4.12	2.29
P	–	11.92	–	12.91	–	17.09
Cr	0.61	1.88	0.64	1.14	0.45	0.55
Mn	–	0.53	–	–	–	0.39
Fe	63.97	64.40	64.00	58.07	39.50	28.92
Ni	33.99	21.27	32.72	27.89	55.93	50.73

substrate material during the non-vacuum electron beam cladding process. The presence of silicides in the coating may contribute to enhanced resistance to high-temperature exposure due to the potential formation of an SiO_2-containing oxide, which exhibits excellent protective properties [23, 24].

Figure 6 displays the X-ray diffraction patterns of the single-layer and multi-layer coatings. The XRD patterns revealed that all coatings comprised a γ-FeNi solid solution, where iron atoms substitute nickel atoms within the lattice. In addition, the triple-layer coating also contained $Fe_{1.8}Ni_{1.2}P$ phosphide and $FeSi_2$ iron silicide phases.

Figure 7a illustrates the oxidation kinetics curves for the initial 0.4 wt.% C-Cr steel (used as a reference) and the cladded coatings at 850°C for 100 hours. The high-temperature oxidation resistance of the materials was evaluated based on the magnitude of the mass gain. During heating of the 0.4 wt.% C-Cr steel, intense oxidation was observed, accompanied by the active formation of an oxide scale that provided no protective effect and did not impede the mutual diffusion of metal and oxygen. The mass gain for the 0.4 wt.% C-Cr steel was 60.81 mg/cm^2. The mass gain for the single-layer, double-layer, and triple-layer coatings was 17.87 mg/cm^2, 11.22 mg/cm^2, and 7.01 mg/cm^2, respectively. Consequently, the triple-layer coating exhibited the greatest oxidation resistance, surpassing that of the 0.4 wt.% C-Cr steel by a factor of 8.7.

Figure 7b presents the XRD patterns of the coatings after isothermal oxidation. The results indicated the formation of iron oxides (Fe_2O_3 and Fe_3O_4) and spinel $NiFe_2O_4$. This

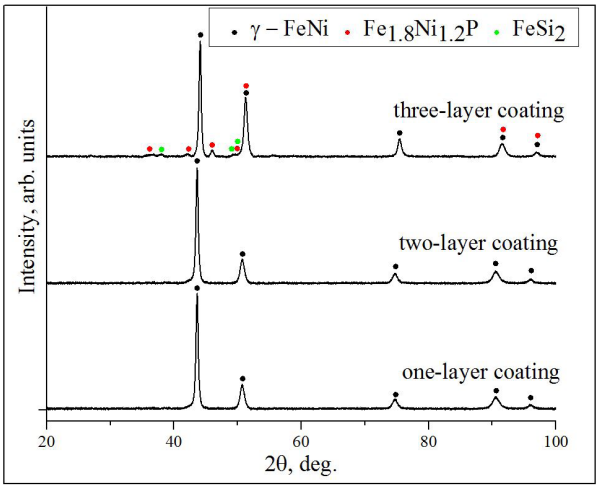

Fig. 6. X-Ray diffraction patterns of nickel coatings formed on 0.4 wt.% C-Cr steel.

complex oxide based on nickel and iron provides better protection against oxygen and metal diffusion [25].

In conclusion, all fabricated coatings enhanced the high-temperature oxidation resistance of the substrate steel due to the formation of spinel. However, the triple-layer coating demonstrated superior performance, owing to the reduced iron concentration within the coating.

The oxide scale thickness was 90 μm for the single-layer coating, 65 μm for the double-layer coating, and 45 μm for the triple-layer coating.

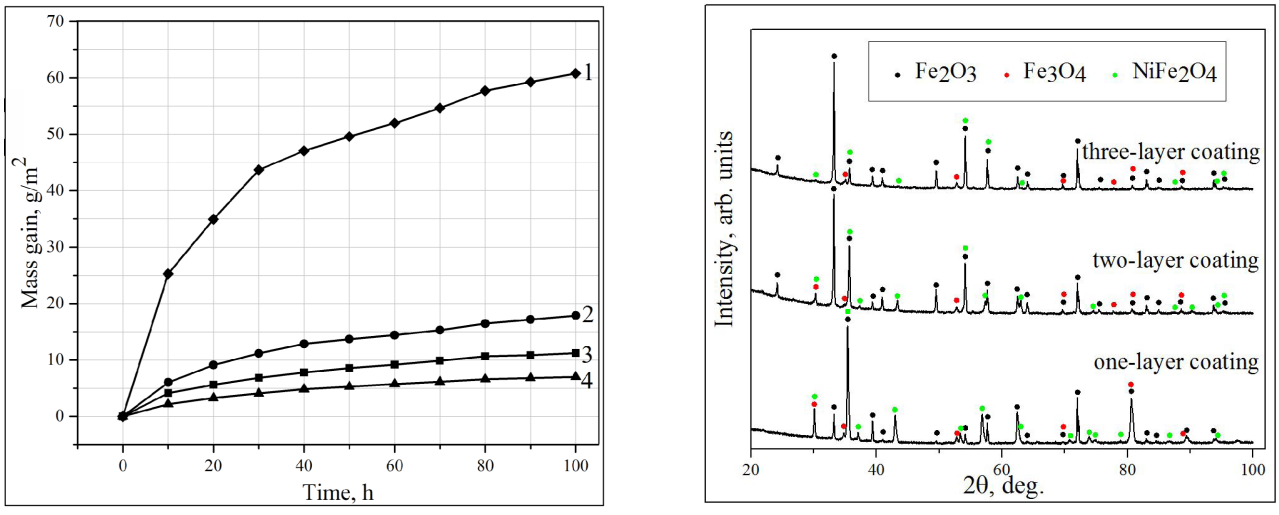

Fig. 7. (Color online) Mass gain curves of the samples as a function of time during oxidation testing at 850°C for 100 hours (a): 1 — substrate, 2 — one-layer coating, 3 — two-layer coating, 4 — three-layer coating; X-ray diffraction patterns of the surfaced coatings following isothermal oxidation at 850°C for 100 hours (b).

The surface morphology of the samples after 100 hours of exposure at 850°C is presented in Fig. 8.

The surface of the 0.4 wt.% C-Cr steel after isothermal oxidation is shown in Fig. 8 a, b, c. The scale comprised iron oxides (Fe_2O_3 and Fe_3O_4). Cracks and high porosity were observed, contributing to rapid oxidation. Delamination was evident on the oxide scale of the single-layer coating (Fig. 8 d, e, f), associated with the formation of various oxides, including iron-nickel spinels (Fig. 8 e) and iron oxides (Fig. 8 f), as confirmed by X-ray diffraction analysis. The surface of the double-layer coating oxide scale (Fig. 8 g, h, i) was homogeneous, but a crack was noted, which may be attributable to thermal stresses [26]. Energy-dispersive X-ray (EDX) analysis revealed the presence of silicon within the coating oxide scale, in addition to iron oxides and spinel, which is believed to reduce the oxidation rate. The triple-layer coating oxide scale exhibited delamination (Fig. 8 j, k, l). A complex oxide scale morphology was observed, with boron, iron, silicon, and nickel present, as determined by EDX analysis. Plate-like features were observed, representing nickel oxide (Fig. 8 k), along with iron oxides and spinel-type oxides (Fig. 8 l).

4. Conclusions

In conclusion, the studies carried out made it possible to establish the optimal value of the current of non-vacuum electron beam surfacing of Colmonoy-227F powder on

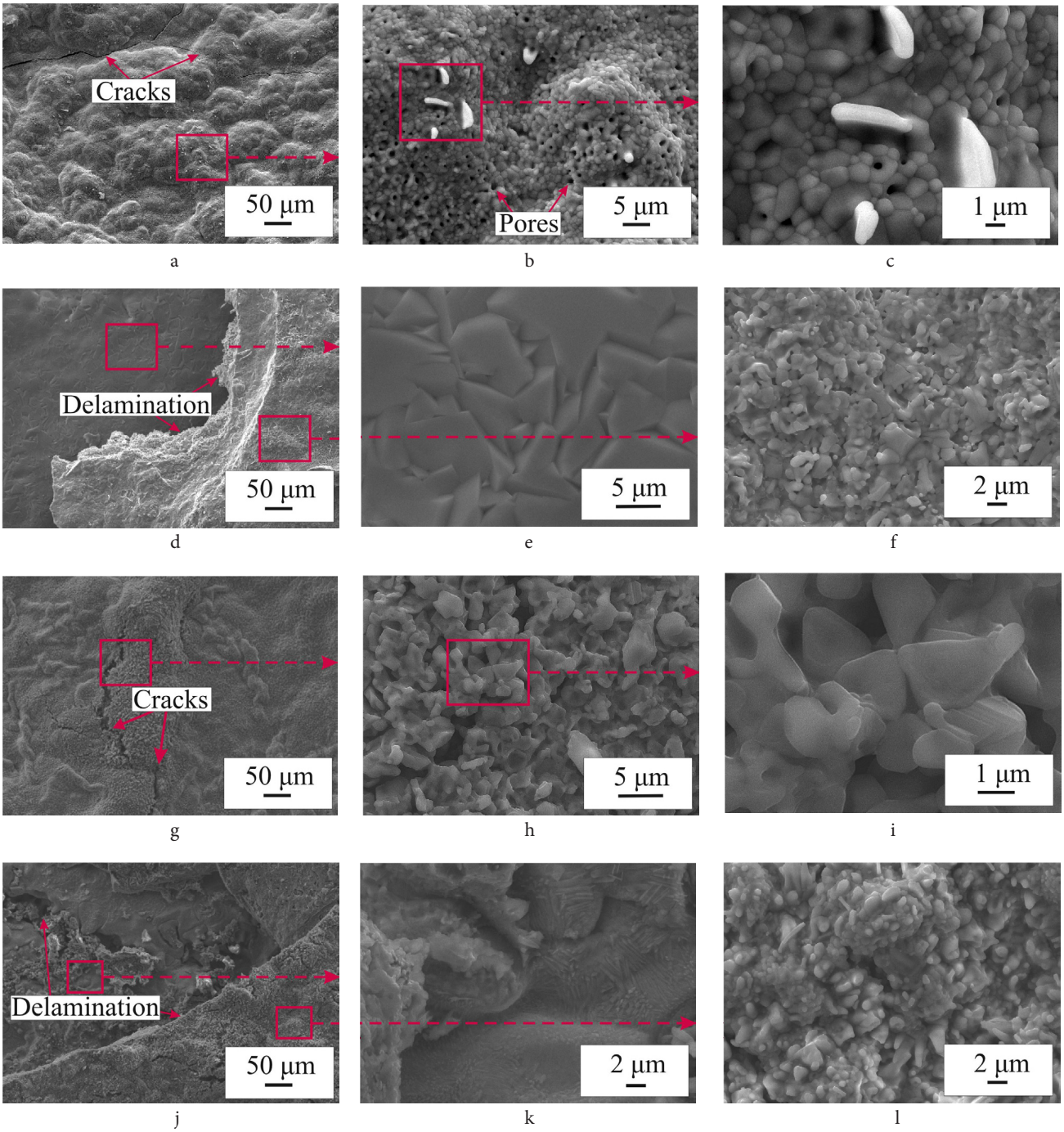

Fig. 8. Surface morphology of cladded coatings and steel after isothermal oxidation at 850°C for 100 hours: 0.4 wt.% C-Cr steel (a, b, c); single-layer coating (d, e, f); double-layer coating (g, h, i); triple-layer coating (j, k, l). Top view.

40X steel, which is equal to 23 mA. At this parameter value, the formation of high-quality alloyed coatings was achieved, both for single-layer and double-layer claddings. The triple-layer coating, however, exhibited defects in the form of porosity and cracks, which were associated with the formation of brittle phases.

The resulting single-layer (2.7 mm thick) and double-layer (3.4 mm thick) coatings possessed a dendritic structure and consisted primarily of a γ-FeNi solid solution. The triple-layer coating (4.4 mm thick) also contained $Fe_{1.8}Ni_{1.2}P$ and $FeSi_2$.

The high-temperature oxidation resistance studies demonstrated that all fabricated alloyed layers provided enhanced oxidation resistance compared to the initial 0.4 wt.% C-Cr steel reference material. The single-layer coating showed a 3.4-fold improvement in oxidation resistance, while the double-layer and triple-layer coatings showed 6-fold and 8.7-fold improvements, respectively.

X-ray phase analysis of the oxidized surfaces revealed the formation of Fe_3O_4, Fe_2O_3, and $NiFe_2O_4$. The improved resistance to high-temperature exposure was attributed to the formation of protective iron-nickel spinel. Furthermore, the presence of silicon was detected in the oxide scale of the double-layer coating, and boron and nickel were additionally detected in the triple-layer coating, indicating a more complex composition and potentially improved protective properties.

In conclusion, the multi-layer coatings based on Colmonoy-227F represent a promising approach for enhancing the operational performance of materials under high-temperature conditions.

References

1. G.-H. Kwon, H. Park, B. Choi, Y.-K. Lee, K. Moon, Influence of Cr Content on the High-Temperature Oxidation Behavior and Mechanism of Low-Alloy Steels, Materials 16 (2023) 4964.
2. M. Mugale, A. Choudhari, S. Karki, J. Desai, G. Walunj, V.B. Vukkum, D. Schwam, R.K. Gupta, T. Borkar, Investigation of Protective Coatings for Reducing High-Temperature Oxidation of Steels, JOM 77 (2025) 653 – 664.
3. M.E. Aalamialeagha, S.J. Harris, M. Emamighomi, Influence of the HVOF spraying process on the microstructure and corrosion behaviour of Ni-20%Cr coatings, Journal of Materials Science 38 (2003) 4587 – 4596.
4. M. Kumar, H. Singh, N. Singh, Production of Nanocrystalline Ni-20Cr Coatings for High-Temperature Applications, J Therm Spray Tech 23 (2014) 692 – 707.
5. R. Haugsrud, On the high-temperature oxidation of nickel, Corrosion Science 45 (2003) 211– 235.
6. D. Tejero-Martin, M. Rezvani Rad, A. McDonald, T. Hussain, Beyond Traditional Coatings: A Review on Thermal-Sprayed Functional and Smart Coatings, J Therm Spray Tech 28 (2019) 598 – 644.
7. L. Ułanowicz, A. Dudziński, Heat-Resistant Protective Coatings Applied to Aircraft Turbine Blades by Supersonic Thermal Spraying and Diffusion-Aluminizing, Coatings 14 (2024) 1554.
8. V.M. Gusev, O.Yu. Elagina, A.G. Buklakov, Improving the Properties of Plasma Heat-Resistant Coatings by Means of Spraying Materials That React with Exothermic Effects, Inorg. Mater. Appl. Res. 13 (2022) 728 – 731.
9. A.N. Cherepanov, A.M. Orishich, V.E. Ovcharenko, A.G. Malikov, V.O. Drozdov, A.P. Pshenichnikov, Influence of Modifying Nanoadditives on the Properties of a Multilayer Composite Coating Obtained by Laser Surfacing, Phys. Metals Metallogr. 120 (2019) 101–106.
10. A.K. Das, A review on coating with high entropy alloy developed by laser energy based surfacing process, Materials Today: Proceedings 52 (2022) 1551–1557.
11. J. Lei, C. Shi, S. Zhou, Z. Gu, L.-C. Zhang, Enhanced corrosion and wear resistance properties of carbon fiber reinforced Ni-based composite coating by laser cladding, Surface and Coatings Technology 334 (2018) 274 – 285.
12. A. Śliwa, J. Mikuła, K. Gołombek, T. Tański, W. Kwaśny, M. Bonek, Z. Brytan, Prediction of the properties of PVD/CVD coatings with the use of FEM analysis, Applied Surface Science 388 (2016) 281 – 287.
13. S. Koseki, K. Inoue, S. Morito, T. Ohba, H. Usuki, Comparison of TiN-coated tools using CVD and PVD processes during continuous cutting of Ni-based superalloys, Surface and Coatings Technology 283 (2015) 353 – 363.
14. A. Thakur, S. Gangopadhyay, K.P. Maity, S.K. Sahoo, Evaluation on Effectiveness of CVD and PVD Coated Tools during Dry Machining of Incoloy 825, Tribology Transactions 59 (2016) 1048 –1058.
15. T.A. Krylova, Yu.A. Chumakov, Fabrication of Cr-Ti-C composite coating by non-vacuum electron beam cladding, Materials Letters 274 (2020) 128022.
16. I.A. Bataev, A.A. Bataev, M.G. Golkovsky, A.Yu. Teplykh, V.G. Burov, S.V. Veselov, Non-vacuum electron-beam boriding of low-carbon steel, Surface and Coatings Technology 207 (2012) 245 – 253.
17. P.F. You, X. Zhang, H.L. Zhang, C.L. Zeng, Oxidation Behavior of $NiFe_2O_4$ Spinel-Coated Interconnects in Wet Air, Oxid Met 90 (2018) 499 – 513.
18. A.A. Ruktuev, D.V. Lazurenko, T.S. Ogneva, R.I. Kuzmin, M.G. Golkovski, I.A. Bataev, Structure and oxidation behavior of CoCrFeNiX (where X is Al, Cu, or Mn) coatings obtained by electron beam cladding in air atmosphere, Surface and Coatings Technology 448 (2022) 128921.
19. I.A. Bataev, D.V. Lazurenko, M.G. Golkovskii, A.A. Bataev, O.E. Matts, Surface Hardening of Titanium Under Non-Vacuum Electron-Beam Cladding of an Aluminum-Containing Powder Mixture, Metal Science and Heat Treatment, 60 (9) (2019) 619 – 624.
20. D.V. Lazurenko, M.G. Golkovsky, A. Stark, F. Pyczak, I.A. Bataev, A.A. Ruktuev, I.S. Laptev, Structure and properties of Ti-Al-Ta and Ti-Al-Cr cladding layers fabricated on titanium, Metals, 11 (7) (2021) 1139.
21. C. Zhang, Y. Zhou, C. Shi, H. Zhou, C. Shen, H. Yu, X. Yuan, W. Ren, H. Lu, Y. Zhong, Z. Lei, T. Zheng, P.K. Liaw, Study on the dendritic growth and grain boundary formation in the suddenly expanded cross-section of single crystal superalloy during directional solidification process,

Journal of Manufacturing Processes 127 (2024) 764 – 778.
22. S. A. Grashkov, M. A. Korovin, E. V. Sazonov, Residual Stresses and Their Stability Under Thermal Exposure, Modern Materials, Equipment, and Technologies: Proceedings of the 12th International Scientific and Practical Conference (Kursk, 2022), pp. 120 –124.
23. Y. Zhang, M. Zhang, G. Zhang, Q. Liu, M. Huang, Y. Lan, P. Feng, Microstructure and Antioxidative Performance of Y_2O_3-CeO_2 Co-Modified Molybdenum Silicide Coatings, Coatings 15 (3) (2025) 310.
24. M. Spalik, Analysis of coatings with Al and Si additives for high-temperature oxidation of steel, JoE360, 1 (1/24) (2024) 35 – 38.
25. L. Ma, K. Zhou, Z. Li, Q. Wei, L. Zhang, Hot corrosion of a novel NiO/$NiFe_2O_4$ composite coating thermally converted from the electroplated Ni-Fe alloy, Corrosion Science 53 (2011) 3712 – 3724.
26. Yu. N. Malyutina, E. A. Pukhova, A. A. Dudareva, B. B. Batyrov, D. V. Lazurenko, I. A. Bataev, Ni-Cr-Ti and Ni-Cr-Ti-B coatings prepared by nonvacuum electron beam cladding: Effect of boron and chromium on the microstructure, hardness and high-temperature oxidation resistance, Materials Today Communications 43 (2025) 111730.